

See discussions, stats, and author profiles for this publication at: <https://www.researchgate.net/publication/233755115>

Interplay between Chemical and Magnetic Order in FeRh Clusters

ARTICLE *in* THE JOURNAL OF PHYSICAL CHEMISTRY C · AUGUST 2012

Impact Factor: 4.77 · DOI: 10.1021/jp3032176

CITATIONS

9

READS

56

2 AUTHORS:



Junais Mekkath

National Institute for Materials Science

13 PUBLICATIONS 45 CITATIONS

SEE PROFILE



G. M. Pastor

Universität Kassel

178 PUBLICATIONS 2,729 CITATIONS

SEE PROFILE

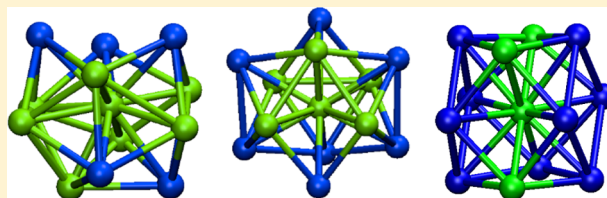
Interplay between Chemical and Magnetic Order in FeRh Clusters

Junais Habeeb Mokkalath and G. M. Pastor*

Institut für Theoretische Physik, Universität Kassel, Heinrich Plett Strasse 40, D-34132 Kassel, Germany

S Supporting Information

ABSTRACT: The structure, chemical order, and magnetic behavior in small FeRh clusters having $N \leq 19$ atoms have been investigated theoretically. For $N \leq 6$ atoms, a thorough global geometry optimization is performed by considering all possible cluster topologies, while for $7 \leq N \leq 19$ only a few representative structures are considered. In all cases, the starting structures are fully relaxed in the entire range of concentrations and spin polarizations. The calculations are based on a generalized-gradient approximation to density-functional theory. The results are analyzed systematically as a function of size and composition. The optimized cluster structures are compact with a clear tendency to maximize the number of nearest-neighbor FeRh pairs. For very small sizes, the low-lying isomers present usually a topology different from that of the optimal structure, while for larger clusters the lowest-energy isomerizations imply mainly changes in the chemical order. The most stable structures are in general ferromagnetic. Antiparallel spin arrangements are found in some low-lying isomers. An important enhancement of the local Fe moments is observed as result of Rh doping. This is shown to be a consequence of an increase in the number of Fe d holes due to Fe–Rh charge transfer. The local moments at the Rh atoms, which are significant already in small pure Rh clusters, are not strongly enhanced by Fe doping. Nevertheless, the overall stability of magnetism, as measured by the energy gained upon spin polarization, increases with Fe content. The influence of spin–orbit interactions on the cluster stability and spin order is discussed.



1. INTRODUCTION

In past decades, the size and structural dependence of the electronic and magnetic properties of nanoscale atomic clusters have been studied systematically. At the beginning, the emphasis has been mainly on clusters of a single element. However, more recently, the interest in alloys, in particular on binary-alloy clusters, has been growing steadily. One of the motivations underlying this development is the search for new materials for specific technological purposes. Indeed, combining elements with complementary or contrasting properties has always been an important route for optimizing the properties of compounds and for discovering new effects and functionalities. Moreover, the perspectives of tailoring the physical behavior are much more diverse in small particles than in condensed matter, due to the possibility of controlling the system size and thus the surface to volume ratio. Consequently, the experimental and theoretical investigations of nanoalloys are a subject of fundamental importance.

The study of magnetic materials is particularly challenging in this context, because it offers numerous ways of exploring competing behaviors.^{1–16} For example, clusters of 3d transition metals (TMs) such as Fe_N , Co_N , and Ni_N show strong average spin moments per atom, as well as enhanced orbital moments and MAEs, which are all significantly larger than in the corresponding periodic solids.^{17–23} In contrast, clusters of 4d and 5d elements show weaker spin polarizations, which decrease rapidly with increasing cluster size, and finally vanish at relatively small sizes [e.g., $\bar{\mu}(\text{Rh}_N) \simeq 0$ for $N \geq 50$ atoms].^{24–28} Therefore, small 3d/4d and 3d/5d alloy particles

are expected to show very interesting size- and concentration-dependent magnetic properties. Another characteristic of TMs is that 4d and 5d elements show stronger spin–orbit (SO) interactions than do the lighter 3d elements. It would be therefore very interesting to investigate to what extent alloying may stabilize magnetism in the 4d and 5d atoms to optimize the MAE, as was already shown in the case of CoRh clusters.²⁹ In this relation, it is important to recall that the magnetic moments and magnetic order resulting from itinerant d electrons depend very strongly on the local environment of the atoms. Therefore, the chemical order within the alloy nanoparticles and the interplay between surface and interface effects should play an important role in defining the magnetic behavior. Conversely, the energetic ordering of the low-lying structures should also depend on the actual magnetic state of the whole cluster, for example, on the total spin polarization. One concludes that the magnetic and chemical orders in these itinerant-electron systems should be investigated on the same footing.

From an experimental perspective, nanoalloys open new ways of designing nanostructured magnetic materials in a bottom-up approach. Still, controlling their composition, size, and magnetic behavior poses serious practical difficulties. Different growth or synthesis conditions can lead to different chemical orders, which can be governed by simple energetics or by more complex kinetic processes. For instance, one may have

Received: April 4, 2012

to deal with segregated clusters having a 4d core and a 3d outer shell or vice versa. Postsynthesis manipulations can induce a variety of structural rearrangements such as order–disorder transitions, intermixing, or surface segregation. Moreover, the resulting bond-length relaxations are expected to depend on size, composition, and the local environment of the atoms. This implies an additional local-symmetry lowering, which is not possible in bulk alloys and which can be important for the interpretation of experiments.

The purpose of this Article is to investigate the structure, chemical order, and magnetic order of small FeRh clusters by using first-principles density-functional theory.³⁰ Besides the general interest of 3d–4d nanomagnetism, FeRh clusters are particularly attractive due to the remarkable temperature–pressure phase diagram observed in FeRh bulk alloys.³¹ In macroscopic Fe₅₀Rh₅₀, the magnetic order at normal pressure and low temperatures is antiferromagnetic (AF). As the temperature increases, this α'' phase undergoes a first-order transition to a ferromagnetic (FM) state, the α' phase, which is accompanied by a change in lattice parameter. The corresponding transition temperature $T_c^{\alpha''\alpha'}$ increases rapidly with increasing external pressure P , eventually displacing the FM α' phase completely for $P \geq 7$ GPa ($T_c^{\alpha''\alpha'} \simeq 290$ K for Fe₅₀Rh₅₀ at normal pressure). This effect disappears in Fe-rich alloys, because $T_c^{\alpha''\alpha'}$ decreases very rapidly with decreasing Rh content. The properties of FeRh bulk alloys have also been the subject of first principles and model theoretical investigations. In particular, it has been shown that the relative stability of the FM and AF solutions depends strongly on the interatomic distances.³² These condensed-matter results provide an additional specific motivation for studying FeRh nanoalloys.

The remainder of this Article is organized as follows. In section 2, the theoretical background is briefly presented. Further details concerning the structural sampling and optimization strategies may be found in ref 33. The results of our calculations are presented and discussed in section 3. The interplay between structure, chemical order, and magnetism is analyzed in the most stable clusters for different sizes and compositions. Finally, section 4 provides a summary of the main trends and an outlook to future extensions.

2. COMPUTATIONAL ASPECTS

In this work, we explore the ground-state energy landscape of FeRh clusters having $N \leq 19$ atoms by performing first principles electronic calculations based on density functional theory.³⁰ To this aim, the Vienna ab initio simulation package (VASP) has been used.³⁴ The exchange and correlation energy is described by using Perdew and Wang's generalized-gradient approximation (GGA).³⁵ For the sake of comparison, calculations have also been performed with the spin-polarized local density approximation (LDA). The VASP solves the Kohn–Sham (KS) equations in an augmented plane-wave basis set, taking into account the core electrons within the projector augmented wave (PAW) method.³⁶ This is an all-electron frozen-core approach, which allows one to incorporate efficiently the nodes of the valence KS orbitals in the core region, and the resulting effects on the electronic structure, total energy, and interatomic forces. The wave functions of the 4s and 3d electrons of Fe, and the 5s and 4d electrons of Rh, are expanded in a plane wave basis set with an energy cutoff $E_{\text{max}} = 268$ eV. A simple cubic supercell is used with the usual periodic boundary conditions. The linear size of the cell is $a = 10$ – 22 Å, so that any pair of images of the clusters are well

separated and the interaction between them is negligible. The PAW sphere radii for Fe and Rh are 1.302 and 1.402 Å, respectively. To speed up convergence, the discrete energy levels are broadened by using a Gaussian smearing $\sigma = 0.02$ eV. Because we are considering finite systems, the reciprocal space summations are restricted to the Γ point.

The validity of the present choice of computational parameters has been verified by performing a number of tests concerning the numerical accuracy. Increasing the cutoff energy, for example, from $E_{\text{max}} = 268$ eV to $E_{\text{max}} = 500$ eV and the supercell size from $a = 12$ Å to $a = 22$ Å yields total energy differences in Rh₄ of about 2 and 0.3 meV, respectively. The corresponding changes in the average bond length and bond angle amount to 10^{-3} Å and 10^{-4}° . These small differences do not affect our conclusions. In fact, typical isomerization energies in these clusters are an order of magnitude larger, approximately 10–30 meV. We also found that the total energy is nearly independent of the choice of the smearing parameter σ , provided that it is not too large ($\sigma \leq 0.05$ eV). Values from $\sigma = 0.01$ to 0.1 eV have been explicitly checked. One concludes that the set of parameters E_{max} , a , and σ mentioned above offers a sufficiently good accuracy at a reasonable computational cost.

One of the central difficulties in the theoretical study of binary-metal particles is the diversity of geometrical conformations and internal distributions of the different atomic species within the clusters, which should be explored to identify the low-energy configurations reliably. This includes various ordered and disordered structures showing different degrees of intermixing or segregation. On the one side, one needs to consider a large, most possibly complete and unbiased set of initial cluster geometries or topologies. On the other side, all possible chemical orders, that is, all distributions of the Fe and Rh atoms, should be taken into account for each cluster size, composition, and structure. Finally, for each initial topology and chemical order, the structures need to be relaxed in a fully unconstrained way until an equilibrium configuration with vanishing interatomic forces is reached.

For clusters having $N \leq 6$ atoms, we have considered all possible topologies and all different distributions of the Fe and Rh atoms within the cluster. This is achieved by generating all possible graphs for $N \leq 6$ atoms as described in ref 37. (See also ref 33.) Despite this very large number of different initial configurations, the unconstrained relaxations using the VASP lead to only relatively few geometries, which can be regarded as stable or metastable isomers. For larger clusters ($7 \leq N \leq 19$), such a thorough enumerative search becomes unfeasible. Therefore, instead of performing a detailed global optimization, we intend to explore the trends as a function of composition and chemical order for a few topologies that are representative of open- and close-packed structures. Taking into account our results for smaller sizes, and the available information on the structure of pure Fe_N and Rh_N clusters, we have restricted the set of starting topologies as follows. For $N = 7$, we consider the bicapped trigonal bipyramid, capped octahedra, and the pentagonal bipyramid. For $N = 8$, we take into account the tricapped trigonal bipyramid, bicapped octahedra, capped pentagonal bipyramid, and cube. Finally, for $N = 13$ and 19, we focus on cuboctahedra (CUBO), hexagonal close packed (HCP), face-centered cubic (FCC), icosahedra (ICO), and simple cubic (SC) structures. This choice is motivated by previous results for pure clusters and by the trend to compact geometries observed for FeRh clusters with $N \leq 6$. Although far

from exhaustive, the considered geometries allow one to explore various relevant growth patterns with a reasonable computational effort. Certainly, a more complete study would be necessary to draw rigorous conclusions about the optimal structures.

The dependence on concentration is investigated systematically for each topology of Fe_mRh_n by varying m and for each size $N = m + n \leq 19$, including the pure Fe_N and Rh_N limits. Moreover, we take into account all possible nonequivalent distributions of the m Fe and n Rh atoms within the cluster. In this way, rigorous information on the chemical order is derived. The atomic positions are fully relaxed without imposing any symmetry constraints,³⁴ until all of the force components are smaller than a threshold of 5 meV/Å. The convergence criterion for the atomic displacements is 5×10^{-4} Å. This procedure applies to all considered clusters. The diversity of the considered geometrical structures and atomic arrangements yields many different local minima, sometimes differing by small distortions and total energies.

Lattice structure and magnetic behavior are intimately related in TMs, particularly in weak ferromagnets such as Fe and its alloys.³⁸ On the one side, the optimum structure and chemical order depend on the magnetic state of the cluster as given by the average magnetic moment per atom $\bar{\mu}_N$ and the magnetic order. On the other side, the magnetic behavior is known to be different for different structures and concentrations. Therefore, to obtain rigorous results on FeRh clusters, we have varied systematically the value of the total spin polarization of the cluster S_z by performing fixed spin-moment (FSM) calculations in the whole physically relevant range.³⁹ In practice, we start from the nonmagnetic state ($S_z^{\text{min}} = 0$) and increase S_z until the local spin moments are fully saturated, that is, until the Fe moments in the PAW sphere reach $\mu_{\text{Fe}} \simeq 4 \mu_B$ and the Rh moments $\mu_{\text{Rh}} \simeq 2.5 \mu_B$ (typically, $S_z^{\text{max}} \gtrsim 3N/2$). The most stable structural and magnetic configuration of Fe_mRh_n correspond to energy minimum as a function of S_z and of the atomic positions.

Once the optimization with respect to structural and magnetic degrees of freedom is achieved, we derive the binding energy per atom $E_B = [mE(\text{Fe}) + nE(\text{Rh}) - E(\text{Fe}_m\text{Rh}_n)]/N$ by referring the total energy E to the corresponding energy of m Fe and n Rh isolated atoms. For each stationary point of the total energy surface (i.e., for each relaxed structure having a nearly vanishing $\|\nabla E\|$), we determine the vibrational frequencies from the diagonalization of the dynamical matrix. In this way, we rule out saddle points to which the local optimization may converge. Only configurations that correspond to true minima are discussed in the following. Finally, a number of electronic and magnetic properties are derived: the magnetic energy $\Delta E_m = E(S_z = 0) - E(S_z)$, the local magnetic moments μ_i integrated within the PAW sphere or Bader atomic cells of atom i ,^{40,41} and the spin polarized density of electronic states (DOS) $\rho_\sigma(\epsilon)$.




3. RESULTS AND DISCUSSION

In this section, we investigate the ground-state structure, chemical order, and magnetic behavior of Fe_mRh_n clusters having $N = m + n \leq 19$ atoms. The main emphasis is here on understanding how the various electronic and magnetic properties depend on the size and the chemical composition of the alloy. First, we consider the smaller clusters ($N \leq 6$) for which all possible topologies have been taken into account. Subsequently, the main trends for larger clusters are

summarized. Analogies and differences in the properties found for the various sizes are discussed.

3.1. FeRh Dimers. Already the dimers allow one to infer very useful trends on the different types of bonds that are found in FeRh alloy clusters. The results summarized in Table 1 show

Table 1. Structural, Electronic, and Magnetic Properties of FeRh Dimers^a

Cluster	Struct.	E_B	ΔE_m	$d_{\alpha\beta}$	$\bar{\mu}_N$	μ_{Fe}	μ_{Rh}	ν_0
Fe_2		1.35	0.77	1.98	3.00	2.82		288
FeRh		1.95	0.24	2.07	2.50	3.34	1.33	359
Rh_2		1.65	0.00	2.21	2.00		1.83	224

^aResults obtained in the GGA are given for the binding energy E_B (in eV), the magnetic stabilization energy $\Delta E_m = E(S_z = 0) - E(S_z)$ (in eV), the average interatomic distance $d_{\alpha\beta}$ (in Å) between atoms α and β ($\alpha, \beta = \text{Fe or Rh}$), the average spin moment per atom $\bar{\mu}_N = 2S_z/N$ (in μ_B), the local spin moment μ_α (in μ_B) at the Fe or Rh atoms, and the vibrational frequency ν_0 (in cm^{-1}).

that the FeRh bond yields the highest cohesive energy, followed by the Rh_2 bond, with the Fe_2 bond being the weakest. The particular strength of the heterogeneous bond is confirmed by the fact that the corresponding vibrational frequency is the highest. The bond length, however, follows the trend of the atomic radii: $d_{\text{RhRh}} > d_{\text{FeRh}} > d_{\text{FeFe}}$. Quantitatively, the binding energy per atom $E_B^{\text{GGA}} = 1.35$ eV obtained for Fe_2 within the GGA is smaller than the LDA result $E_B^{\text{LDA}} = 2.25$ eV,⁴² although it still remains larger than the experimental value $E_B^{\text{expt}} = 0.65$ eV reported in ref 43. The calculated vibrational frequency $\nu_0(\text{Fe}_2) = 288 \text{ cm}^{-1}$ is consistent with previous measurements [$\nu_0(\text{Fe}_2) = 299.6 \text{ cm}^{-1}$ from ref 43 and $\nu_0(\text{Fe}_2) = 300 \pm 15 \text{ cm}^{-1}$ from ref 44]. Our results for E_B and $\bar{\mu}_N$ of Rh_2 coincide with the GGA calculations by Reddy et al.,⁴⁵ which are however larger than the experimental values $E_B^{\text{expt}}(\text{Rh}_2) = 1.46$ eV from Knudsen effusion,⁴⁶ $E_B^{\text{expt}}(\text{Rh}_2) = 0.70 \pm 0.15$ eV from Raman resonance in Ar matrixes,⁴⁷ and $E_B^{\text{expt}}(\text{Rh}_2) = 1.203$ eV from resonant two-photon ionization.⁴⁸ The calculated vibrational frequency of $\nu_0(\text{Rh}_2)^{\text{GGA}} = 224 \text{ cm}^{-1}$ should be compared to the experimental $\nu_0(\text{Rh}_2)^{\text{expt}} = 283.9 \text{ cm}^{-1}$ reported in ref 47.

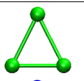
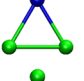
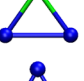
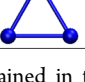
The stability of magnetism can be quantified theoretically by the difference in the total energy ΔE_m between the nonmagnetic ($S_z = 0$) and optimal magnetic solutions. As expected, one observes that ΔE_m is largest for Fe_2 and smallest for Rh_2 . The same trend holds for the average magnetic moment per atom, which decreases linearly from $\bar{\mu}_2 = 3 \mu_B$ to $2 \mu_B$ as one goes from Fe_2 to Rh_2 . This corresponds to a nearly full polarization of all of the d electrons in the PAW spheres: $\nu_d \simeq 7$ for Fe and $\nu_d \simeq 8$ for Rh, where ν_d stands for the calculated number of valence d electrons in the PAW sphere. The local magnetic moments μ_α with $\alpha = \text{Fe and Rh}$, are obtained by integrating the spin density within the PAW spheres, which have the radius $r_0 = 1.3$ Å for Fe and $r_0 = 1.4$ Å for Rh. In the pure dimers, the calculated local moments $\mu_{\text{Fe}} = 2.82 \mu_B$ and $\mu_{\text{Rh}} = 1.83 \mu_B$ are close to the corresponding average moment per atom $\bar{\mu}_2 = 3 \mu_B$ and $2 \mu_B$. This indicates that the spin-density $m(\vec{r}) = n_\uparrow(\vec{r}) - n_\downarrow(\vec{r})$ is quite localized around the atoms. In fact, the difference between μ_α and $\bar{\mu}_N$ gives a measure of the spin density $m(\vec{r})$, which is spilled off the immediate environment of the atoms.

The results for μ_α in the mixed FeRh dimer are quite remarkable, particularly if one compares them to the behavior of pure dimers. Indeed, the Fe local moment in FeRh is

significantly enhanced with respect to Fe_2 , and even with respect to the Fe-atom, while the Rh moment is reduced by a similar amount ($\Delta\mu_{\text{Fe}} = 0.52 \mu_{\text{B}}$ and $\Delta\mu_{\text{Rh}} = -0.50 \mu_{\text{B}}$, see Table 1). This can be explained by a transfer of d electrons from Fe to Rh, which enhances the number of d holes and allows the Fe atom to develop a significantly larger spin moment. This increase of μ_{Fe} occurs at the expense of the moment at the Rh atom, which now has less d holes to polarize. The present interpretation is confirmed by an analysis of the electronic density integrated within the Bader cells,⁴⁰ which shows that in the FeRh dimer, 0.33 electrons are transferred from Fe to Rh. Moreover, this behavior is qualitatively in agreement with the higher Pauling electronegativity χ of the Rh atom ($\chi_{\text{Fe}} = 1.83$ and $\chi_{\text{Rh}} = 2.28$).⁴⁹

3.2. FeRh Trimers. The most stable trimers are found to be triangles for all compositions (see Table 2). According to our

Table 2. Structural, Electronic, and Magnetic Properties of FeRh Trimers^a

Cluster	Struct.	E_{B}	ΔE_{m}	$d_{\alpha\beta}$	$\bar{\mu}_{\text{N}}$	μ_{Fe}	μ_{Rh}	ν_0
Fe_3		1.80	0.69	2.22	3.33	2.99		267
Fe_2Rh		2.24	0.32	$\begin{smallmatrix} 2.25 \\ 2.35 \end{smallmatrix}$	3.00	3.35	1.21	235
FeRh_2		2.45	0.05	$\begin{smallmatrix} 2.21 \\ 2.57 \end{smallmatrix}$	2.00	3.27	1.18	287
Rh_3		2.31	0.02	2.37	1.00		0.93	210

^aResults obtained in the GGA are given for the binding energy per atom E_{B} (in eV), the magnetic stabilization energy per atom $\Delta E_{\text{m}} = [E(S_z = 0) - E(S_z)]/N$ (in eV), the average interatomic distance $d_{\alpha\beta}$ (in Å) ordered from top to bottom as d_{FeFe} , d_{FeRh} , and d_{RhRh} , the average spin moment per atom $\bar{\mu}_{\text{N}} = 2S_z/N$ (in μ_{B}), the local spin moment μ_{α} (in μ_{B}) at the Fe or Rh atoms, and the lowest vibrational frequency ν_0 (in cm^{-1}).

calculations, the ground state of Rh_3 is equilateral with local magnetic moments $\mu_{\alpha} = 0.93 \mu_{\text{B}}$, which align parallel to each other and are almost as large as $\bar{\mu}_3$. These results are consistent with previous GGA studies of Rh_3 which yield $E_{\text{B}} = 2.35$ eV, $d = 2.45$ Å, and $\bar{\mu}_3 = 1 \mu_{\text{B}}$.⁴⁵ The substitution of a Rh atom gives an isosceles FeRh_2 with the Rh atoms forming the longer side. Notice that the bond-length $d_{\text{RhRh}} = 2.57$ Å is larger than in Rh_3 . The linear isomer of the form Rh-Fe-Rh , that is, with only FeRh bonds, lies 0.4 eV above the optimal structure. This is the only true local minimum among the linear FeRh trimers. The other linear structures (i.e., Rh-Rh-Fe , Fe-Rh-Fe , and Fe-Fe-Rh) are all found to be saddle points connecting triangular local minima of the potential energy surface (PES). Further, Fe substitution yields a isosceles Fe_2Rh in which the FeFe bond is the shortest. One observes, as in the dimers, that the interatomic distances follow the trends in the atomic radii. Finally, for Fe_3 , the lowest-energy structure calculated in the GGA is a Jahn–Teller distorted isosceles triangle with two longer bonds ($d_{12} = d_{13} = 2.30$ Å) and a much shorter one ($d_{23} = 2.07$ Å). These results coincide with previous GGA studies⁵⁰ predicting $d_{12} = d_{13} = 2.33$ Å and $d_{23} = 2.09$ Å. In contrast, the LDA result reported in ref 42 is an equilateral triangle with average magnetic moment $\bar{\mu}_3 = 2.66 \mu_{\text{B}}$ and $d = 2.10$ Å. We have repeated the calculations by using the spin-polarized LDA,


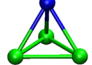
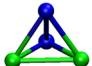


and otherwise the same computational parameters as for the GGA, and also obtained an equilateral triangle similar to the one reported in ref 42. One concludes that exchange and correlation effects are so important in this case that the precise approximation changes the geometry qualitatively. Furthermore, we have analyzed the GGA Kohn–Sham spectrum in the equilateral structure and found a high degeneracy at the Fermi energy, which justifies the interpretation that the distortion is triggered by a Jahn–Teller effect. Concerning the composition dependence of E_{B} , one observes a nonmonotonous behavior as for $N = 2$, which indicates that the FeRh bonds are the strongest. The lowest vibrational frequency follows a similar trend, despite the larger mass of Rh. Notice that FeRh_2 is somewhat more stable than Fe_2Rh , because the bonds between Rh atoms are in general stronger than those between Fe atoms.

The average magnetic moment per atom in Rh_3 amounts to $1 \mu_{\text{B}}$. In the alloys, it increases monotonously with Fe doping, reaching $\bar{\mu}_3 = (10/3)\mu_{\text{B}}$ for Fe_3 . The local magnetic moments μ_{α} in the PAW spheres always show a FM-like coupling. They are all identical in Rh_3 and close to $\bar{\mu}_3$, which is consistent with the C_3 point-group symmetry. The value of the local moment $\mu_{\text{Rh}} = 0.93 \mu_{\text{B}}$ is very close to the average total moment $\bar{\mu}(\text{Rh}_3) = 1 \mu_{\text{B}}$. This shows that the spin polarization is dominated by electrons occupying localized states and that spill off contributions are not important. In the case of Fe_3 , one finds $\mu_1 = 3.23 \mu_{\text{B}}$ and $\mu_2 = \mu_3 = 2.87 \mu_{\text{B}}$ in the PAW spheres, the latter corresponding to the pair of atoms forming the shorter bond. For mixed compositions, as soon as FeRh bonds are present, the local Fe moments are enhanced beyond $3 \mu_{\text{B}}$. As in the dimer, this is mainly due to a charge transfer from Fe to Rh, which increases the number of Fe d holes. Quantitatively, the local μ_{Fe} and μ_{Rh} in mixed trimers are similar to the values found in the FeRh dimer, although somewhat smaller. In addition, one observes an enhancement of the Rh local moments in Fe_2Rh and FeRh_2 as compared to pure Rh_3 . This reflects the importance of the proximity of Fe on the magnetic behavior of Rh atoms. Finally, one should also mention that the energy gain ΔE_{m} associated with magnetism only plays a quantitative role in the relative stability of triangular and linear FeRh trimers. ΔE_{m} is actually larger for the linear chain than for the triangle. Therefore, the triangles remain the most stable structures even in the nonmagnetic case, although with somewhat different bond lengths.

3.3. FeRh Tetramers. The most stable FeRh tetramers are all tetrahedra, and the first low-lying isomers are rhombi (see Table 3). The distribution of the Fe and Rh atoms within the cluster does not play a role in defining the optimal structure, because in a tetrahedral topology the atoms can be permuted at will without altering the chemical order. In the case of Rh_4 , the ground state is a nonmagnetic undistorted tetrahedron, in agreement with previous studies.⁵¹ The closest isomer is found to be a bent rhombus with an average bond length $d = 2.35$ Å. Notice, however, that Bae et al.⁵² found a bent rhombus as the ground-state structure for Rh_4 by using the same simulation package (VASP). This discrepancy is likely to be a consequence of the different choice of the pseudopotential and cutoff energy E_{max} . In our calculations, we considered the PAW method and $E_{\text{max}} = 268$ eV, while in ref 52, ultrasoft pseudopotentials and $E_{\text{max}} = 205.5$ eV were used.

The concentration dependence of the binding energy is nonmonotonous, as was also found in smaller clusters (see Table 3). This shows that the FeRh bonds remain the strongest. Following the changes in E_{B} from Rh_4 to Fe_4 , one

Table 3. Structural, Electronic, and Magnetic Properties of FeRh Tetramers as in Table 2

Cluster	Struct.	E_B	ΔE_m	$d_{\alpha\beta}$	$\bar{\mu}_N$	μ_{Fe}	μ_{Rh}	v_0
Fe ₄		2.21	0.35	2.28	3.50	3.08		279
Fe ₃ Rh		2.49	0.58	2.34 2.40	3.00	3.18	1.03	232
Fe ₂ Rh ₂		2.74	0.37	2.52 2.31 2.72	2.50	3.39	1.03	243
FeRh ₃		2.76	0.21	2.30 2.60	1.75	3.25	1.12	289
Rh ₄		2.75	0.00	2.45	0.00		0.00	201


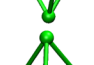
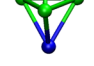


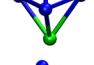
may qualitatively correlate the relative stability of the clusters to the number of homogeneous and heterogeneous bonds. For instance, FeRh₃, which is the most stable composition, has 3 FeRh and 3 RhRh bonds. Replacing a Rh by a Fe to obtain Fe₂Rh₂ implies replacing 2 RhRh bonds by a somewhat stronger FeRh bond and a weaker FeFe bond. Thus, E_B does not change significantly. Only for larger Fe content is a clear decrease of E_B observed. It is worth noting that these trends are not altered qualitatively when magnetism is neglected, that is, if one considers E_B for $S_z = 0$.

The average magnetic moment $\bar{\mu}_N$ increases approximately linearly with Fe content. In general, the substitution of a Rh atom by an Fe atom changes the total moment $2S_z$ by 3 or 4 μ_B , or equivalently, $\Delta\bar{\mu}_N = (0.75-1) \mu_B$ (see Table 3). The magnetic order is always FM-like, and the local moments in the alloys are appreciably larger than those in the pure clusters. This can be traced back to a d-electron charge transfer from Fe to Rh. In addition, the presence of Fe in Fe_mRh_n enhances the Rh local moments particularly with respect to pure Rh₄, which is paramagnetic.

3.4. FeRh Pentamers. Although all possible cluster topologies were considered as starting geometries for each composition, only the most highly coordinated trigonal bipyramid (TBP) and the square pyramid (SP) are found to be the most stable geometries (see Table 4). In fact, most of the low coordinated structures transform into compact structures after the unconstrained local relaxation. Except for Rh₅, the optimal structure of which is a SP, all of the other FeRh pentamers have the TBP as ground-state geometry. The trend in the composition dependence of the binding energy E_B of pentamers is somewhat different from the case of dimers and trimers, as we started to observe for $N = 4$. Indeed, in the Fe-rich limit E_B increases rapidly with increasing Rh content, as the weakest FeFe bonds are replaced by FeRh bonds. However, near 50% concentration and in the Rh-rich limit, the composition dependence is weak, because FeRh and RhRh bonds are now comparably strong (see Table 4).

The structure obtained for Rh₅, a square pyramid, coincides qualitatively with previous DFT calculations.⁴⁵ Nevertheless, we obtain a binding energy that is 0.07 eV per atom lower than in ref 45. Substituting one Rh atom by Fe yields FeRh₄ and changes the optimal cluster topology to the more compact TBP. The SP remains a local minimum, which is only 3 meV per atom less stable than the optimal TBP geometry. The average magnetic moment $\bar{\mu}(\text{FeRh}_4) = 1.2 \mu_B$ is enhanced with

Table 4. Structural, Electronic, and Magnetic Properties of FeRh Pentamers as in Table 2

Cluster	Struct.	E_B	ΔE_m	$d_{\alpha\beta}$	$\bar{\mu}_N$	μ_{Fe}	μ_{Rh}	v_0
Fe ₅		2.51	1.00	2.41	3.20	2.93		227
Fe ₄ Rh		2.76	1.01	2.30 2.47	3.00	3.09	1.06	243
Fe ₃ Rh ₂		2.96	0.92	2.37 2.39	2.40	3.13	0.75	244
Fe ₂ Rh ₃		3.06	0.55	2.35 2.71	2.20	3.36	1.08	260
FeRh ₄		3.01	0.33	2.39 2.51	1.20	3.31	0.57	251
Rh ₅		3.03	0.70	2.48	1.00		0.95	113

respect to Rh₅ due to the contribution of a particularly large Fe local moment $\mu_{Fe} = 3.31 \mu_B$. Notice that the Rh moments are no longer enhanced, as is often found in the smaller FeRh_{N-1}, but significantly reduced to $\mu_{Rh} = 0.62 \mu_B$ for the apex atoms and $\mu_{Rh} = 0.52 \mu_B$ for the Rh atoms sharing a triangle with the Fe. This is a consequence of the relatively low value of the ground-state S_z . The effect is even stronger in the SP isomer of FeRh₄. Here, we find two Rh moments $\mu_{Rh} = 0.43 \mu_B$, which couple parallel to the Fe moment, a very small $\mu_{Rh} = 0.05 \mu_B$, and an antiparallel $\mu_{Rh} = -0.48 \mu_B$. Consequently, a reduced average total moment $\bar{\mu}_S = 0.8 \mu_B$ and a very small average Rh moment $\mu_{Rh} = 0.15 \mu_B$ are obtained. This example illustrates the subtle competition between cluster structure and magnetism in 3d–4d nanoalloys.

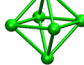
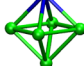
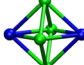
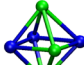
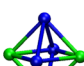
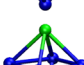
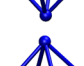
Further increase in the Fe content does not change the topology of the optimal structure. Moreover, for nearly equal concentrations of Fe and Rh (i.e., Fe₂Rh₃ and Fe₃Rh₂), one starts to see that the low-lying isomers are the result of changes in the chemical order. In other words, the bottom of the PES is dominated by changes in the distribution of the Fe and Rh atoms within the cluster, rather than by changes in the cluster topology. In the most stable configuration of Fe₂Rh₃ (Fe₃Rh₂), the 3 Rh (Fe) atoms are all NNs of each other (see Table 4). This is understandable from a single-particle perspective, because the band energy is lower when orbitals having nearly the same energy levels are multiply hybridized. In addition, the optimal structures maximize first the number of FeRh NN pairs, followed by the number of RhRh pairs.⁵³ Finally, in the Fe-rich limit, for example, in Fe₄Rh, the lowest-energy structure remains a TBP, but the closest isomer corresponds to the SP, that is, a different topology rather than a different chemical order.

The trends in the magnetic properties are dominated by the Fe content, because $\bar{\mu}_N$ increases monotonously with Fe concentration. The first excited isomers show the same $\bar{\mu}_N$ as the optimal structure except for FeRh₄, where an antiparallel alignment of Rh local moments is found. The enhancement of

the local Fe moments is stronger for Rh-rich clusters, because the FeRh charge transfer is somewhat larger (see Table 4). In contrast, the substitution of Rh by Fe does not always enhance the Rh local moments, as we observed systematically for smaller sizes. Finally, it is interesting to observe that the different chemical orders found in the low-lying isomers of Fe_2Rh_3 and Fe_3Rh_2 correspond to different local magnetic moments. The environment dependence of μ_α follows in general the trend of higher spin polarization at the lowest coordinated sites.¹⁷

3.5. FeRh Hexamers. Despite the wide variety of the considered starting topologies and chemical orders, most low coordinated structures relax into compact ones in the course of the unconstrained relaxations (see section 2). In the end, the square bipyramid (SBP), in general somehow distorted, yields the lowest energy regardless of composition (see Table 5). The

Table 5. Structural, Electronic, and Magnetic Properties of FeRh Hexamers as in Table 2

Cluster	Struct.	E_B	ΔE_m	$d_{\alpha\beta}$	$\bar{\mu}_N$	μ_{Fe}	μ_{Rh}	V_0
Fe_6		2.74	1.03	2.38	3.33	2.95		206
Fe_5Rh		2.94	1.07	2.38 2.46	3.16	3.10	1.20	210
Fe_4Rh_2		3.14	0.85	2.38 2.45	3.00	3.28	1.22	214
Fe_3Rh_3		3.21	0.56	2.62 2.38 2.61	2.50	3.32	1.14	239
Fe_2Rh_4		3.26	0.38	2.46 2.51	2.33	3.38	1.39	207
FeRh_5		3.24	0.28	2.44 2.54	1.83	3.37	1.33	192
Rh_6		3.20	0.19	2.54	1.00		0.91	188

binding energy per atom E_B shows a composition dependence similar to that for pentamers. For Fe-rich clusters, E_B increases by about 0.2 eV each time a Rh replaces a Fe (see Table 5). However, for nearly equal concentrations and in Rh-rich clusters ($\text{Fe}_{6-n}\text{Rh}_n$ with $n \geq 4$), E_B becomes almost independent of n . This seems to be the result of competing bonding and magnetic contributions. In fact, the magnetic energy ΔE_m continues to decrease with increasing Rh content, by about 0.1–0.2 eV per Rh substitution, even for high Rh content. This is compensated by an increase of the bonding energy with increasing n .

In the case of Rh_6 , a regular octahedron yields the lowest energy. The first isomer, a trigonal prism (TP), lies only 28 meV above the optimum, showing a somewhat shorter average bond length $d = 2.46$ Å and a higher average moment $\bar{\mu}_6 = 1.67 \mu_B$. These results are consistent with previous DFT calculations.⁵⁴ A single Fe substitution enhances the average moment to $\bar{\mu}_6 = 1.83 \mu_B$ but does not change the topology of FeRh_5 . The RhRh distances remain essentially unchanged, and

the FeRh distances are somewhat shorter. The important increase in the ground-state spin polarization ($5 \mu_B$ in all) is not only due to the larger Fe moment ($\mu_{\text{Fe}} = 3.37 \mu_B$ in the PAW sphere) but also results from the enhancement of the local Rh moments ($\mu_{\text{Rh}} = 1.33 \mu_B$, see Table 5). The first isomer of FeRh_5 corresponds to a distorted trigonal prism with significantly contracted FeRh and RhRh bond lengths. In Fe_2Rh_4 , the Fe atoms occupy the opposite apex positions of the octahedron. In this way, each Fe is 4-fold coordinated with all Rh atoms, thus maximizing the number of FeRh bonds. The local Fe moments in Fe_2Rh_4 are the largest among all hexamers: $\mu_{\text{Fe}} = 3.38 \mu_B$, slightly beyond the value found in FeRh_5 . In addition, important spin polarizations are induced at the neighboring Rh atoms ($\mu_{\text{Rh}} = 1.39 \mu_B$). The first isomer of Fe_2Rh_4 corresponds to a capped trigonal bipyramid (CTBP) having a short FeFe bond. This structure lies only 0.11 eV above the optimal one and has the same total moment. Replacing a further Fe atom yields Fe_3Rh_3 , whose structure is an octahedron having two isosceles Fe_3 and Rh_3 triangles forming a $\pi/2$ angle with respect to each other (see Table 5). Out of the 12 NN pairs in the Fe_3Rh_3 octahedron, 8 are FeRh and only 4 are homogeneous (2 FeFe and 2 RhRh). The local Fe magnetic moments are similar to the other clusters, but the Rh moments are somewhat smaller on average ($\mu_{\text{Rh}} = 1.14 \mu_B$). The first excited isomer of Fe_3Rh_3 is a CTBP that lies 25 meV per atom above the ground state. For Fe_4Rh_2 , the lowest-energy structure is also an octahedron, while a distorted CTBP is a local minimum lying 0.14 eV per atom above the ground state. In the former, the Rh atoms are far apart occupying the apical positions, whereas in the latter they are NNs. The situation is thus similar to what we find in Fe_3Rh_2 . As one further reduces the Rh content, the octahedron and a distorted CTBP remain the two most stable structures (see Table 5 for Fe_5Rh and Fe_6). Notice that for low Rh or Fe concentrations, the atoms are distributed to favor the FeRh bonds rather than homogeneous NN pairs between the atoms in the minority.

The main trends in the magnetic properties are in many respects qualitatively similar to the behavior found in smaller sizes. This concerns in particular the increase of $\bar{\mu}_N$ and ΔE_m with increasing Fe concentration, the small differences in $\bar{\mu}_N$ between the low-lying isomers, the dominant role of the local d-electron spin polarization, the enhancement of the Fe moments upon Rh doping, and the stabilization of the Rh moments by the proximity of the Fe atoms. One may further notice that μ_{Rh} is always larger in the FeRh hexamers than in pure Rh_6 . However, this is not valid for all N , because the magnetic moments in small Rh clusters are also enhanced due to the extremely reduced coordination numbers.

3.6. Exploring Larger Clusters. For Fe_mRh_n clusters having $m + n = N \geq 7$, we do not aim to perform a full global structure optimization but rather to investigate the interplay between chemical order and magnetism systematically and as a function of composition. Therefore, only a few representative topologies are considered as a starting point of the unconstrained local minimizations. The precise list of structures is given in section 2. For each nanoalloy, all possible distributions of the Fe and Rh atoms, and all relevant values of the total magnetization S_z , are explored, from the nonmagnetic state to saturation. Thus, the trends on chemical order and magnetic behavior remain rigorous within the framework of the sampled topologies.

As shown in Table 6, the PBP is the most stable structure of Rh_7 among the considered starting geometries. This result is

Table 6. Structural, Electronic, and Magnetic Properties of FeRh Heptamers^a

Cluster	Struct.	E_B	ΔE_m	$d_{\alpha\beta}$	$\bar{\mu}_N$	μ_{Fe}	μ_{Rh}	v_0
Fe ₇		2.95	0.84	2.47	3.14	2.88		209
Fe ₆ Rh		3.11	0.78	2.51 2.43	3.00	2.98	1.17	226
Fe ₅ Rh ₂		3.25	0.73	2.45 2.46	2.86	3.12	1.19	236
Fe ₄ Rh ₃		3.36	0.62	2.42 2.55 2.71	2.71	3.27	1.26	222
Fe ₃ Rh ₄		3.38	0.57	2.48 2.37 2.67	2.28	3.25	1.16	218
Fe ₂ Rh ₅		3.41	0.45	2.40 2.62	2.14	3.34	1.33	205
FeRh ₆		3.37	0.28	2.52 2.57	1.71	3.20	1.29	220
Rh ₇		3.33	0.22	2.61	1.86		1.62	203

^aThe results are obtained from a restricted representative sampling of cluster topologies (see section 2).

consistent with some earlier DFT studies.⁵¹ However, it contrasts with the calculations by Wang et al.,⁵⁴ who used the GGA functional of ref 35 and obtained a capped octahedra, and with the calculations of Bae et al.,⁵² who found a prism plus an atom on a square face. According to our results, these structures are, respectively, 20 and 4 meV per atom less stable than the PBP. Notice that, particularly in the latter case, a 4 meV energy difference is too small to allow drawing definitive conclusions.

FeRh heptamers with high Rh concentrations also favor PBP structures. In FeRh₆ the Fe atom occupies an apex site, while in Fe₂Rh₅ and Fe₃Rh₄ the Fe atoms belong to the pentagonal ring. Moreover, the distances between the two apex atoms in Rh₇ and between the Fe and Rh apex atoms in FeRh₆ are quite short. In contrast, in Fe₂Rh₅ and Fe₃Rh₄ the Fe atoms are as far as possible from each other, and the distance between the Rh apex atoms is larger. These differences are consistent with the previously discussed trend to favor the stronger FeRh bonds. For example, the energy involved in changing the position of the Fe atom in FeRh₆ from the apex (7 FeRh bonds) to the pentagonal ring (5 FeRh bonds) is 16 meV per atom.

As the Fe content increases, the topology of Fe_mRh_n changes. In fact, Fe₄Rh₃ corresponds to a CO, while for $m \geq 5$ the configuration yielding the lowest energy can be regarded as a strongly distorted PBP (see Table 6). Already in Fe₄Rh₃, but also in Fe₅Rh₂, one observes a tendency of the Fe atoms to group in subclusters, bringing the Rh atoms to outer positions, so that the number of FeRh bonds is largest. Concerning the shape of the Fe-rich heptamers, one observes important deformations of the pentagonal bipyramid (D_{5h} symmetry), which are similar to the distortions found in pure Fe₇.^{55,56} While the precise origin of the symmetry lowering is difficult to establish in the alloys, it is reasonable to expect that it is similar to the case of pure Fe₇. According to ref 56, the deformations

found in Fe₇ are due to the presence of degenerate electronic states in the undistorted PBP structure. To verify this hypothesis, we have analyzed the KS spectrum of the symmetric structure (D_{5h} symmetry) and also found that it is highly degenerate at ϵ_F . In contrast, the spectrum of the distorted structure has a band gap of about 0.4 eV at ϵ_F . This suggests that the distortions in Fe-rich alloy clusters can be interpreted as a Jahn–Teller effect.

The results for octamers are summarized in Table 7. The most stable structure obtained for Fe₈ is a bicapped octahedra

Table 7. Structural, Electronic, and Magnetic Properties of FeRh Octamers^a

Cluster	Struct.	E_B	ΔE_m	$d_{\alpha\beta}$	$\bar{\mu}_N$	μ_{Fe}	μ_{Rh}	v_0
Fe ₈		3.03	0.76	2.42	3.00	2.77		209
Fe ₇ Rh		3.19	0.73	2.43 2.47	2.87	2.88	1.04	208
Fe ₆ Rh ₂		3.32	0.66	2.43 2.47	2.75	3.18	1.04	190
Fe ₅ Rh ₃		3.42	0.69	2.43 2.57	2.62	3.15	1.10	189
Fe ₄ Rh ₄		3.47	0.53	2.45 2.42 2.70	2.50	3.20	1.25	197
Fe ₃ Rh ₅		3.54	0.42	2.77 2.39 2.65	2.37	3.36	1.34	214
Fe ₂ Rh ₆		3.53	0.32	2.70 2.59 2.57	2.00	3.25	1.30	208
FeRh ₇		3.49	0.23	2.45 2.57	1.62	3.27	1.18	202
Rh ₈		3.59	0.09	2.40	1.50		1.33	160

^aThe results are obtained from a restricted representative sampling of cluster topologies (see section 2).

(BCO). A similar geometry has been found in previous spin-polarized LDA calculations, which reported $E_B = 4.12$ eV and $\bar{\mu}_8 = 3 \mu_B$.⁵⁷ We have repeated the LDA calculations for the BCO structure with our computational parameters and atomic reference energies and found $E_B = 3.51$ eV. In the other extreme, for pure Rh₈, the optimal structure, among the considered starting topologies, is a regular cube having $E_B = 3.59$ eV, an average magnetic moment $\bar{\mu}_8 = 1.5 \mu_B$, and all bond lengths equal to 2.40 Å. These results are in good agreement with previous calculations by Bae et al.⁵⁸ In this context, it is most interesting to observe that the substitution of a single Rh atom by Fe, in FeRh₇ changes the structure to a compact topology, which is more stable than all of the relatively open relaxed cube-like structures derived from pure Rh₈. The same trend holds for higher Fe content (i.e., Fe_mRh_{8-m} with $m \geq 1$). The dominant structure for nonvanishing Fe content is a BCO with slight distortions (see Table 7). Only for Fe₅Rh₃ do we find a different topology, a distorted capped pentagonal bipyramid. For these compositions, the typical isomerization

energies between the low-lying structures are $\Delta E = 10\text{--}30$ meV per atom.

Concerning the magnetic properties of heptamers and octamers, one observes that in most cases the average magnetic moment per atom $\bar{\mu}_N$ and the magnetic energy ΔE_m increase with Fe concentration. The only exception is the pure Rh heptamer, for which $\bar{\mu}_7$ is somewhat larger than in FeRh_6 . This is not due to an AF-like coupling between Fe impurity moment and the remaining Rh atoms, but rather to a reduction of the Rh local moments in FeRh_6 ($\mu_{\text{Rh}} \approx 1.61\text{--}1.63 \mu_B$ in Rh_7 , while $\mu_{\text{Rh}} \approx 1.25\text{--}1.30 \mu_B$ in FeRh_6). Remarkably, the Rh local moments in Rh_7 are the largest among all of the heptamers. They amount to 87% of the total moment, which stresses the importance of the local d-electron contributions. Also in Rh_8 , with its open cube structure, one finds quite large local moments, which are actually larger than the Rh moments in most Fe doped clusters. This shows that for these sizes, the Fe atoms do not necessarily increase the Rh moments by simple proximity effects (see Tables 6 and 7). Nevertheless, a different behavior is expected for larger N , where pure Rh clusters are no longer magnetic on their own.

The local Fe moments are in general strongly enhanced with respect to pure Fe_N ($\mu_{\text{Fe}} \approx 2.8 \mu_B$ in Fe_7 or Fe_8) reaching values up to $3.36 \mu_B$, particularly when the Fe atoms are in a Rh-rich environment. As in the smaller clusters, this is a consequence of a charge transfer from the Fe to the Rh atoms, which increases the number of polarizable Fe d-holes. Notice that some kind of interaction between the Fe atoms, probably triggered by the large exchange splittings, seems to favor this effect, because the largest μ_{Fe} are found for clusters having 2 or 3 Fe atoms, rather than for the single Fe impurity. Large local Fe moments are also found in bulk FeRh alloys.^{14,62} Let us finally point out that the average magnetic moments in the lowest-lying isomers are either the same or very similar to the ground state.

In Table 8, results are given for clusters having $N = 13$ atoms. The corresponding structures are illustrated in Figure 1. Results

Table 8. Electronic and Magnetic Properties of Fe_mRh_n Clusters Having $m + n = 13$ Atoms^a

cluster	E_B	ΔE_m	$\bar{\mu}_N$	μ_{Fe}	μ_{Rh}	ν_0
Fe_{13}	3.31	0.99	3.38	3.05		364
Fe_{12}Rh	3.38	1.28	3.15	3.00	1.02	340
$\text{Fe}_{11}\text{Rh}_2$	3.46	1.09	2.92	2.95	0.97	319
$\text{Fe}_{10}\text{Rh}_3$	3.53	1.04	2.69	2.93	0.89	301
Fe_9Rh_4	3.60	1.01	2.31	2.80	0.73	291
Fe_8Rh_5	3.68	0.82	2.23	2.88	0.87	305
Fe_7Rh_6	3.72	0.63	2.15	2.94	0.96	332
Fe_6Rh_7	3.76	0.57	2.08	3.00	1.03	310
Fe_5Rh_8	3.77	0.53	2.00	2.38	1.06	302
Fe_4Rh_9	3.78	0.51	1.76	2.99	1.05	290
$\text{Fe}_3\text{Rh}_{10}$	3.82	0.37	1.69	3.03	1.09	301
$\text{Fe}_2\text{Rh}_{11}$	3.84	0.24	1.61	3.06	1.16	319
FeRh_{12}	3.78	0.17	1.54	2.96	1.26	340
Rh_{13}	3.86	0.04	0.54		0.45	281

^aThe corresponding cluster geometries are illustrated in Figure 1.

for $N = 19$ may be found in the Supporting Information. These were obtained by using the following starting topologies: cuboctahedron, icosahedron, hexagonal close packed, face centered cubic, and a cube-like. A number of interesting structural changes are observed as a function of concentration. For Fe_{13} , we obtain an icosahedron, having ferromagnetic order

and a remarkable large $\bar{\mu}_N = 3.38 \mu_B$. These results are in good agreement with previous calculations by Sahoo and co-workers.⁵⁹ The first isomer, among the considered topologies, is a hcp structure lying 90 meV above the optimum and having $\bar{\mu}_N = 3.23 \mu_B$. For a single Rh doping, in Fe_{12}Rh , the optimal shape remains an icosahedron with the Rh atom located at the surface. A drop of only $0.23 \mu_B$ is observed in $\bar{\mu}_N$, as compared to Fe_{13} , despite the much smaller Rh local moment (see Table 8 and Figure 1). The first isomer of Fe_{12}Rh is an hcp-like structure having the Rh atom at the surface, which lies 10 meV above the ground state. In the case of $\text{Fe}_{11}\text{Rh}_2$ and $\text{Fe}_{10}\text{Rh}_3$, the Rh atoms distribute themselves in a way that maximizes the number of FeRh bonds. A first significant structural change is observed for $\text{Fe}_{10}\text{Rh}_3$ in which ground state is hcp-like, followed by a return to the icosahedral shape in Fe_9Rh_4 . For nearly equal concentrations, we identify the hcp structure (Fe_7Rh_6) and fcc structure (Fe_6Rh_7) as the lowest energy configurations. Notice that in all of the lowest energy isomers, the bulk-like central position of the cluster is always occupied by a Fe atom (see Figure 1). Finally, in the case of Rh_{13} , a double cube with an atom adsorbed to a lateral phase and having $\bar{\mu}_N = 0.69 \mu_B$ is the most stable geometry (see Table 8). The first isomer is also a double cube, with an atom capping a square on the top. The energy difference with respect to the ground state is 0.76 meV per atom. The results for Rh_{13} are in good agreement with previous calculations by Bae et al.⁵⁸ As in the smaller clusters, the cubic structure is relevant only for pure Rh clusters.

As the size of the nanoalloy grows, determining the structure and chemical order becomes increasingly demanding, not only because of the increasing cost of the individual electronic calculations, but also due to the growing diversity of atomic arrangement having similar short-range patterns. The risk of getting erroneously trapped close to the initial configuration is therefore important. Similar concerns apply to the magnetic order, particularly in systems showing weak nonsaturated ferromagnetic or antiferromagnetic behavior, as is the case of FeRh compounds. Nevertheless, some qualitative trends can be inferred from our calculations on Fe_mRh_n with $m + n = 19$ atoms as a function of composition. One observes that the cohesive energy per atom increases systematically with increasing Rh content. This increase is first rapid (from $E_B \approx 3.4$ eV/atom in Fe_{19} to $E_B \approx 4.0$ eV/atom in $\text{Fe}_{10}\text{Rh}_9$) as FeFe bonds are replaced by the stronger FeRh bonds. For more than the 50% Rh content, E_B then increases much more slowly (e.g., $E_B \approx 4.1$ eV/atom in $\text{Fe}_m\text{Rh}_{19-m}$ with $m \leq 5$), which suggests that FeRh and RhRh bonding are comparatively strong. The magnetic moment per atom $\bar{\mu}_N$ and the energy gained upon magnetization ΔE_m decrease monotonously with decreasing Fe content. For example, $\bar{\mu}_{19} = 3.1, 2.9, 1.7$, and 0.8 in $\text{Fe}_m\text{Rh}_{19-m}$ with $m = 19, 18, 9$, and 2 , respectively. The magnetic energy amounts to $\Delta E_m = 0.8$ eV/atom in Fe_{19} and Fe_{18}Rh , decreasing progressively to $\Delta E_m = 0.1$ and 0.02 eV/atom in FeRh_{18} and Rh_{19} . The local magnetic moments at the Fe atoms are remarkably stable throughout the whole range of concentrations, showing the already observed slight enhancement in a Rh-rich environment (e.g., $\mu_{\text{Fe}} = 2.8, 2.9, 3.1, 3.0, 3.2, 3.1$ in $\text{Fe}_m\text{Rh}_{19-m}$ with $m = 19, 13, 11, 8, 5$, and 2 , respectively). The corresponding average Rh moments are $\mu_{\text{Rh}} = (0.8\text{--}0.9) \mu_B$ for concentrations up to 50% dropping to $\mu_{\text{Rh}} = (0.4\text{--}0.5) \mu_B$ for $\text{Fe}_m\text{Rh}_{19-m}$ with $m \leq 9$. This excludes the pure Rh_{19} cluster, which is very weakly magnetic ($\bar{\mu}_{19} = 0.06 \mu_B$ and $\mu_{\text{Rh}} = 0.05 \mu_B$ in Rh_{19}).

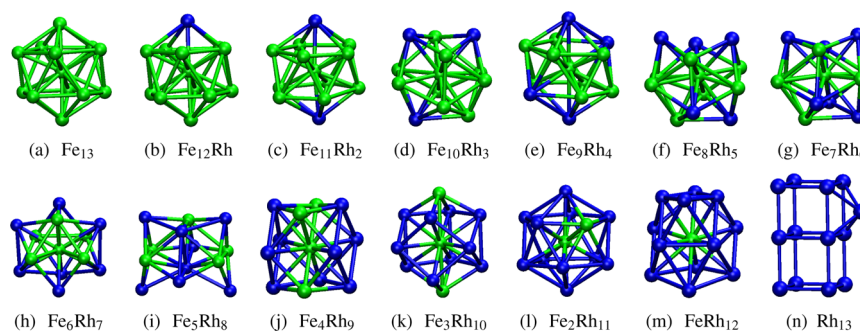


Figure 1. Illustration of the stable structures obtained for $\text{Fe}_m\text{Rh}_{19-m}$ clusters having $m + n = 13$ atoms. Light (dark) spheres represent Fe (Rh) atoms. Only a restricted representative sampling of starting topologies has been considered for the geometry optimization (see section 2).

Concerning the composition dependence of the cluster structures, we observe that the results for pure clusters are very different from those for the nanoalloys. Fe_{19} takes a double icosahedra form with $\bar{\mu}_{19} = 3.05 \mu_B$, in agreement with a recent GGA study.⁶⁰ The calculated $\bar{\mu}$ is quite close to the experimental value $\bar{\mu}_{19} = 2.92 \mu_B$ reported in ref 61. The first isomer is a strongly distorted compact structure, also having $\bar{\mu}_{19} = 3.05 \mu_B$, which is 0.11 eV/atom less stable than the double icosahedron. Rh_{19} shows a simple cubic structure as predicted by Bae et al.⁵⁸ In contrast, for almost all intermediate concentrations ($\text{Fe}_m\text{Rh}_{19-m}$ with $1 \leq m \leq 17$), we observe that the cuboctahedral topology with minor distortions yields the lowest energy. The chemical order in the cuboctahedral structures corresponds to a layered structure with alternating Fe and Rh planes. This behavior can be explained by the trend to maximize the number of heterogeneous FeRh bonds. Finally, one should note that a single Fe impurity is enough to render compact structures more stable than the simple cubic structure, in agreement with the results for smaller sizes.

To conclude this section, it is interesting to compare the cluster results with available experiments and calculations for macroscopic alloys.^{14,62,63} Band structure calculations for the periodic $\text{Fe}_{0.5}\text{Rh}_{0.5}$ alloy having a CsCl structure yield an antiferromagnetic (AF) ground state, which is more stable than the ferromagnetic solution.⁶³ This is qualitatively in agreement with experiments showing AF order when the Rh concentration is above or equal to 50%.⁶² In contrast, our results for small clusters show FM-like order for all Rh concentrations, even for the pure Rh clusters. This is most probably a consequence of the reduction of local coordination number and the associated narrowing of the effective d-bandwidth. Indeed, a narrower d-band renders the Stoner criterion far easier to satisfy and tends to stabilize the high-spin states with respect to the low-spin AF states. In fact, even in bulk FeRh, the energies of the AF and FM states are not very different. A coexistence of both solutions is found over a wide range of volumes.⁶³ Moreover, experiment shows an AF to FM transition with increasing temperature, which is accompanied by an enhanced thermal expansion.⁶² Recent ab initio calculations have revealed the importance of competing FM and AF exchange interactions in stoichiometric α -FeRh.¹⁴

Neutron-diffraction experiments⁶² on $\text{Fe}_{1-x}\text{Rh}_x$ for $0.35 < x < 0.5$ and calculations¹⁴ for $x = 0.5$ show that the Fe local moments μ_{Fe} in the bulk are significantly enhanced with respect to μ_{Fe} in pure α -Fe. Particularly in the FM state μ_{Fe} reaches about $3.2 \mu_B$.^{14,62} These bulk results are remarkably similar to the trends found in Fe_mRh_n clusters over a wide range of compositions. As in the clusters, the induced Rh moments μ_{Rh}

play an important role in the stability of the FM phase. Bulk experiments⁶² on $\text{Fe}_{1-x}\text{Rh}_x$ yield $\mu_{\text{Rh}} \approx 1 \mu_B$ for $0.35 < x < 0.5$, which is comparable to the present cluster results, although somewhat smaller.

4. CONCLUSION

The interplay of magnetic and chemical order in small Fe_mRh_n clusters has been investigated in the framework of a generalized-gradient approximation to density-functional theory. Fully unconstrained structural relaxations have been performed in the entire range of compositions and spin polarizations. A very rich structural and magnetic behavior has been revealed, which is representative of the broader family of 3d–4d nanoalloys. The optimized geometries are in general compact, the alloys showing a strong tendency to intermixing to maximize the number of FeRh nearest-neighbor bonds. For very small sizes, the low-lying isomers usually have a topology different from that of the optimal structure. In larger clusters, the lowest-energy isomerizations imply mainly changes in the chemical order, keeping the underlying topology essentially unchanged. In some cases, the calculations predict very small energy differences, for instance a few meV, among the low-lying isomers. This renders an unambiguous theoretical determination of the ground-state configuration quite difficult. Moreover, it suggests that different chemical orders might coexist in a cluster beam. This could lead to some scatter of the average magnetic moments per atom, because different isomers may show somewhat different magnetic properties. The most stable structures are in general ferromagnetic, although antiparallel spin arrangements were found in some low-lying isomers. The trends in magnetism are controlled to a large extent by the Fe content. For example, the average magnetic moment per atom $\bar{\mu}_N$ and the stability of magnetism, as measured by the energy ΔE_m gained upon spin polarization, generally increase as a function of Fe concentration. In addition, one observes an important enhancement of the local moments at the Fe atoms in a Rh-rich environment due an Fe-to-Rh charge-transfer effect, which increases the number of spin-polarizable 3d holes.

To go beyond the present study, it is interesting to investigate the role of spin–orbit (SO) interactions on the magnetism of 3d–4d nanoalloys. For this purpose, we have calculated the ground-state structure, chemical order, and spin moments of some representative FeRh clusters by including the SO contributions. For example, in Fe_6 , Fe_3Rh_3 , and Rh_6 , we find that the changes in the ground-state energy resulting from SO interactions are typically of the order of 30–40 meV/atom. These values are comparable to, often even larger than, the

energy differences between the low-lying isomers. However, the SO energies are in general very similar for different structures, so that the ground-state structures remain essentially the same as in the scalar relativistic (SR) calculations. Moreover, the changes in the bond lengths d_{ij} and in the average spin moments $\bar{\mu}_S$ resulting from SO coupling are also very small: $|\bar{\mu}_S^{\text{SO}} - \bar{\mu}_S^{\text{SR}}| \simeq 0.01 \mu_B$ and $|d_{ij}^{\text{SO}} - d_{ij}^{\text{SR}}| \simeq 0.001 \text{ \AA}$ in Fe_3Rh_3 . Consequently, the conclusions on the relative stability and spin moments that were drawn from our SR calculations remain valid. In contrast, SO effects are known to be crucial for the magneto-anisotropic behavior, as well as for the orbital contribution to the cluster magnetization. Indeed, a general enhancement of the magnetic anisotropy energy and orbital magnetic moments $\bar{\mu}_L$ has been predicted in pure 3d TM clusters due to their reduced size and symmetry.^{20,64} Moreover, particularly interesting composition-dependent properties are expected in 3d–4d nanoalloys due to the role of the stronger SO interactions at the heavier 4d atoms. As we have seen in this work, the latter are important magnetic components on their own. Further investigations in this direction, on the basis of the structures and the chemical orders reported in previous sections, seem therefore most worthwhile.

■ ASSOCIATED CONTENT

● Supporting Information

Results for the structural, electronic, and magnetic properties of Fe_mRh_n clusters having $m + n = 19$ atoms. This material is available free of charge via the Internet at <http://pubs.acs.org>.

■ AUTHOR INFORMATION

Corresponding Author

*Phone: +49 561 804-4785. Fax: +49 561 804-4006. E-mail: pastor@uni-kassel.de.

Notes

The authors declare no competing financial interest.

■ ACKNOWLEDGMENTS

We thank Dr. J. L. Ricardo-Chávez and Dr. L. Díaz-Sánchez for helpful discussions and useful comments. Computer resources provided by the IT Service Center of the University of Kassel and by the CSC of the University of Frankfurt are gratefully acknowledged.

■ REFERENCES

- (1) See, for instance: Johnston, R. L.; Ferrando, R., Eds. Nanoalloys: From Theory to Applications. *Faraday Discuss.* **2008**, 138, 1.
- (2) Zitoun, D.; Respaud, M.; Fromen, M.-C.; Casanove, M. J.; Lecante, P.; Amiens, C.; Chaudret, B. *Phys. Rev. Lett.* **2002**, 89, 037203.
- (3) Dennler, S.; Ricardo-Chávez, J. L.; Morillo, J.; Pastor, G. M. *Eur. Phys. J. D* **2003**, 24, 237.
- (4) Efremenko, I.; Sheintuch, M. *Chem. Phys. Lett.* **2005**, 401, 232–240.
- (5) Ganguly, S.; Kabir, M.; Datta, S.; Sanyal, B.; Mookerjee, A. *Phys. Rev. B* **2008**, 78, 014402.
- (6) Entel, P.; Gruner, M. E. *J. Phys.: Condens. Matter* **2009**, 21, 064228.
- (7) Andriotis, A. N.; Mpourmpakis, G.; Froudakis, G. E.; Menon, M. *J. Chem. Phys.* **2004**, 120, 11901.
- (8) Rollmann, G.; Sahoo, S.; Hucht, A.; Entel, P. *Phys. Rev. B* **2008**, 78, 134404.
- (9) Bansmann, J.; Baker, S.; Binns, C.; Blackman, J.; Buecher, J.-P.; Dorantes-Dávila, J.; Dupuis, V.; Favre, L.; Kechrakos, D.; Kleibert, A.; et al. *Surf. Sci. Rep.* **2005**, 56, 189.

- (10) Antoniak, C.; Lindner, J.; Spasova, M.; Sudfeld, D.; Acet, M.; Farle, M.; Fauth, K.; Wiedwald, U.; Boyen, H.-G.; Ziemann, P.; et al. *Phys. Rev. Lett.* **2006**, 97, 117201.
- (11) Yin, S.; Moro, R.; Xu, X.; de Heer, W. A. *Phys. Rev. Lett.* **2007**, 98, 113401.
- (12) Knickelbein, M. B. *Phys. Rev. B* **2007**, 75, 014401.
- (13) Wang, R. M.; Dmitrieva, O.; Farle, M.; Dumpich, G.; Ye, H. Q.; Poppa, H.; Kilaas, R.; Kisielowski, C. *Phys. Rev. Lett.* **2008**, 100, 017205.
- (14) Gruner, M. E.; Rollmann, G.; Entel, P.; Farle, M. *Phys. Rev. Lett.* **2008**, 100, 087203.
- (15) Sun, Y.; Zhang, M.; Fournier, R. *Phys. Rev. B* **2008**, 77, 075435.
- (16) Sun, Y.; Fournier, R.; Zhang, M. *Phys. Rev. A* **2009**, 79, 043202.
- (17) Tournus, F.; Tamion, A.; Blanc, N.; Hannour, A.; Bardotti, L.; Prével, B.; Ohresser, P.; Bonet, E.; Epicier, T.; Dupuis, V. *Phys. Rev. B* **2008**, 77, 144411.
- (18) Pastor, G. M.; Dorantes-Dávila, J.; Bennemann, K. H. *Physica B* **1988**, 149, 22; *Phys. Rev. B* **1989**, 40, 7642.
- (19) Bucher, J. P.; Douglass, D. C.; Bloomfield, L. A. *Phys. Rev. Lett.* **1991**, 66, 3052.
- (20) Douglass, D. C.; Bucher, J. P.; Bloomfield, L. A. *Phys. Rev. B* **1992**, 45, 6341.
- (21) Douglass, D. C.; Cox, A. J.; Bucher, J. P.; Bloomfield, L. A. *Phys. Rev. B* **1993**, 47, 12874.
- (22) Billas, I. M. L.; Becker, J. A.; Châtelain, A.; de Heer, W. A. *Phys. Rev. Lett.* **1993**, 71, 4067.
- (23) Billas, I. M. L.; Châtelain, A.; de Heer, W. A. *Science* **1994**, 265, 1682.
- (24) Pastor, G. M.; Dorantes-Dávila, J.; Pick, S.; Dreyssé, H. *Phys. Rev. Lett.* **1995**, 75, 326.
- (25) Apsel, S. E.; Emmert, J. W.; Deng, J.; Bloomfield, L. A. *Phys. Rev. Lett.* **1996**, 76, 1441.
- (26) Knickelbein, M. B. *Phys. Rev. Lett.* **2001**, 86, 5255.
- (27) Nicolas, G.; Dorantes-Dávila, J.; Pastor, G. M. *Phys. Rev. B* **2006**, 74, 014415.
- (28) Galicia, R. *Rev. Mex. Fis.* **1985**, 32, 51.
- (29) Dorantes-Dávila, J.; Dreyssé, H.; Pastor, G. M. *Phys. Rev. B* **1992**, 46, 10432.
- (30) Cox, A. J.; Louderback, J. G.; Bloomfield, L. A. *Phys. Rev. Lett.* **1993**, 71, 923.
- (31) Cox, A. J.; Louderback, J. G.; Apsel, S. E.; Bloomfield, L. A. *Phys. Rev. B* **1994**, 49, 12295.
- (32) Reddy, B. V.; Khanna, S. N.; Dunlap, B. I. *Phys. Rev. Lett.* **1993**, 70, 3323.
- (33) Villaseñor-González, P.; Dorantes-Dávila, J.; Dreyssé, H.; Pastor, G. M. *Phys. Rev. B* **1997**, 55, 15084.
- (34) Muñoz-Navia, M.; Dorantes-Dávila, J.; Zitoun, D.; Amiens, C.; Jaouen, N.; Rogalev, A.; Respaud, M.; Pastor, G. M. *Appl. Phys. Lett.* **2009**, 95, 233107.
- (35) Hohenberg, P.; Kohn, W. *Phys. Rev.* **1964**, 136, B864.
- (36) Kohn, W.; Sham, L. J. *Phys. Rev.* **1965**, 140, A1133.
- (37) Massalski, T. B.; Murray, J. L.; Bennett, L. H.; Baker, H. *Binary Alloy Phase Diagrams*; American Society for Metals: Metals Park, OH, 1986; Vol. 1.
- (38) Gruner, M. E.; Hoffmann, E.; Entel, P. *Phys. Rev. B* **2003**, 67, 064415.
- (39) Mokkath, J. H.; Pastor, G. M. *Phys. Rev. B* **2012**, 85, 054407.
- (40) Kresse, G.; Furthmüller, J. *Phys. Rev. B* **1996**, 54, 11169.
- (41) Kresse, G.; Joubert, D. *Phys. Rev. B* **1999**, 59, 1758.
- (42) Kresse, G.; Lebacqz, O. *VASP Manual*; <http://cms.mpi.univie.ac.at/vasp/>.
- (43) Perdew, J. P.; Chevary, J. A.; Vosko, S. H.; Jackson, K. A.; Pederson, M. R.; Singh, D. J.; Fiolhais, C. *Phys. Rev. B* **1992**, 46, 6671.
- (44) Blöchl, P. E. *Phys. Rev. B* **1994**, 50, 17953.
- (45) Pastor, G. M.; Hirsch, R.; Mühlischlegel, B. *Phys. Rev. Lett.* **1994**, 72, 3879; *Phys. Rev. B* **1996**, 53, 10382.
- (46) For a discussion of the interplay between electron correlations, structure, and magnetism of small clusters, see, for example, refs 17 and 37.
- (47) Let us recall that $S_z = (\nu_\uparrow - \nu_\downarrow)/2$, where ν_\uparrow (ν_\downarrow) stands for the number of electrons having majority (minority) spin.
- (48) Bader, R. F. W. *Atoms in Molecules, A Quantum Theory*; Oxford University Press: Oxford, 1990.

- (41) Ricardo-Chávez, J. L. Ph.D. Thesis, Université Paul Sabatier, Toulouse, France, 2007.
- (42) Castro, M.; Salahub, D. R. *Phys. Rev. B* **1994**, *49*, 11842. Chien, C. H.; Blaisten-Barojas, E.; Pederson, M. R. *Phys. Rev. A* **1998**, *58*, 2196. Chen, J. L.; Wang, C. S.; Jackson, K. A.; Pederson, M. R. *Phys. Rev. B* **1991**, *44*, 6558. Cox, D. M.; Trevor, D. J.; Whetten, R. L.; Rohlfing, E. A.; Kaldor, A. *Phys. Rev. B* **1985**, *32*, 7290.
- (43) Moskovits, M.; Dilella, D. P. *J. Chem. Phys.* **1980**, *73*, 4917.
- (44) Leopold, D. G.; Linenger, W. C. *J. Chem. Phys.* **1986**, *85*, 51.
- (45) Reddy, B. V.; Nayak, S. K.; Khanna, S. N.; Rao, B. K.; Jena, P. *Phys. Rev. B* **1999**, *59*, 5214.
- (46) Cocke, D. L.; Gingerich, K. A. *J. Chem. Phys.* **1974**, *60*, 1958.
- (47) Wang, H.; Haouari, H.; Craig, R.; Lui, Y.; Lombardi, J. R.; Lindsay, D. M. *J. Chem. Phys.* **1997**, *106*, 2101.
- (48) Langenberg, J. D.; Morse, M. D. *J. Chem. Phys.* **1998**, *108*, 2331.
- (49) Pauling, L. *J. Am. Chem. Soc.* **1932**, *54*, 3570.
- (50) Gutsev, G. L.; Khanna, S. N.; Jena, P. *Phys. Rev. B* **2000**, *62*, 1604. Chrétien, S.; Salahub, D. R. *Phys. Rev. B* **2002**, *66*, 155425.
- (51) Futschek, T.; Marsman, M.; Hafner, J. *J. Phys. C. M.* **2005**, *17*, 5927.
- (52) Bae, Y.-C.; Osanai, H.; Kumar, V.; Kawazoe, Y. *Phys. Rev. B* **2004**, *70*, 195413.
- (53) The optimal Fe₃Rh₂ structure has 6 FeRh and 3 FeFe NN pairs, while the first isomer has 5 FeRh, 3 FeFe, and 1 RhRh NN pairs. The optimal Fe₂Rh₃ structure has 6 FeRh and 3 RhRh NN pairs, while the first isomer has 6 FeRh, 2 RhRh, and 1 FeFe NN pairs.
- (54) Wang, L.; Ge, Q. *Chem. Phys. Lett.* **2002**, *366*, 368–376.
- (55) Ballone, P.; Jones, R. O. *Chem. Phys. Lett.* **1995**, *233*, 632.
- (56) Rollmann, G.; Entel, P.; Sahoo, S. *Comput. Mater. Sci.* **2005**, *35*, 275.
- (57) Diéguez, O.; Alemany, M. M. G.; Rey, C.; Ordejón, P.; Gallego, L. *J. Phys. Rev. B* **2001**, *63*, 205407.
- (58) Bae, Y.-C.; Kumar, V.; Osanai, H.; Kawazoe, Y. *Phys. Rev. B* **2005**, *72*, 125427.
- (59) Sahoo, S.; Hucht, A.; Gruner, M. E.; Rollmann, G.; Entel, P.; Postnikov, A.; Ferrer, J.; Fernández-Seivane, L.; Richter, M.; Fritsch, D.; Sil, S. *Phys. Rev. B* **2010**, *82*, 054418.
- (60) Datta, S.; Kabir, M.; Dasgupta, T. S. *Phys. Rev. B* **2011**, *84*, 075429.
- (61) Knickelbein, M. B. *Chem. Phys. Lett.* **2002**, *353*, 221.
- (62) Shirane, G.; Nathans, R. *Phys. Rev.* **1964**, *134*, A1547–A1553.
- (63) Moruzzi, V. L.; Marcus, P. M. *Phys. Rev. B* **1992**, *46*, 2864.
- (64) Guirado-López, R.; Dorantes-Dávila, J.; Pastor, G. M. *Phys. Rev. Lett.* **2003**, *90*, 226402.